Acta Oceanol. Sin., 2019, Vol. 38, No. 4, P. 20–28
https://doi.org/10.1007/s13131-019-1409-3
http://www.hyxb.org.cn
E-mail: hyxbe@263.net

Eddy generation mechanism in the eastern South China Sea

Jiajia Chen[1], Xuhua Cheng[1, 2*], Xiao Chen[1]

[1] College of Oceanography, Hohai University, Nanjing 210098, China

[2] Key Laboratory of Coastal Disaster and Defence (Hohai University), Ministry of Education, Nanjing 210098, China

Received 14 June 2018; accepted 20 August 2018

Abstract

Mesoscale eddy generation mechanisms in the eastern South China Sea (ESCS) are investigated using altimetry observations and solutions of a nonlinear, 1½-layer reduced-gravity model. We estimate the relative roles of the wind forcing in the interior South China Sea (SCS) and the remote forcing from the western tropical Pacific (WTP) in eddy generation in the ESCS. Model solutions show that the high-frequency wind in the interior SCS is the primary forcing for eddies, which explains about 54% of the mesoscale eddies generated in the ESCS. Signals from the WTP also play an important role. Wind-driven equatorial signals reach the west coast of Luzon Island through the Sibutu Passage and Mindoro Strait. The reflected Rossby waves from the west coast of Luzon Island propagate westward, become unstable, and turn into eddies. The signals driven by high-frequency wind from the WTP explain about 40% of the mesoscale eddies generated in the ESCS. The high-frequency wind forcing in both the SCS and the WTP is important for eddy generation in the ESCS.

Key words: mesoscale eddy, South China Sea, wind forcing, Rossby wave

Citation: Chen Jiajia, Cheng Xuhua, Chen Xiao. 2019. Eddy generation mechanism in the eastern South China Sea. Acta Oceanologica Sinica, 38(4): 20–28, doi: 10.1007/s13131-019-1409-3

1 Introduction

The South China Sea (SCS) is the largest semi-enclosed marginal sea in the western tropical Pacific (WTP). There are many passages connecting the SCS with the Pacific Ocean, Java Sea and Sulu Sea. The Luzon Strait is a wide and deep pathway, which enables water exchange between the WTP and the SCS. The SCS also receives influence from the WTP through the Mindoro Strait (Liu et al., 2011; Zhuang et al., 2013; Cheng et al., 2016). The monsoon plays an important role in the surface circulations of the SCS (Wyrtki, 1961; Fang et al., 1998; Qu, 2000; Wang et al., 2006; Liu et al., 2008). The complicated dynamic environment in and around the SCS results in abundant mesoscale eddies in the SCS.

1.1 *Features of mesoscale eddies in the SCS*

The development of satellite altimetry has provided a new way to identify and explore spatio-temporal distribution of mesoscale eddies in the SCS. Based on five-year altimetry data, Wang et al. (2000) revealed two significant mesoscale variability bands in the SCS. The northern band is in the SW–NE direction extending from the Luzon Strait to the Vietnam coast; the southern one lies along the western boundary. Similar patterns were also found by Cheng and Qi (2010) and Zhuang et al. (2010).

Many literatures discussed the main features of eddy activities in the SCS (e.g., Hwang and Chen, 2000; Wang et al., 2003; Su, 2004; Yuan et al., 2007; Cheng et al., 2010; Xiu et al., 2010; Chen et al., 2011; Zu et al., 2013). Chen et al. (2011) showed the mean eddy features in the SCS. They found that almost three in five mesoscale eddies in the SCS have radii of 100–200 km and an average lifetime of about 62 d. Eddy radius near 9°N is very close to the Rossby radius of deformation, but the radius decreases toward the equator. It remains unknown why eddies in the southern SCS have relatively small radius.

Mesoscale eddies in the SCS have distinct seasonal variability. More cyclonic eddies (CEs) are generated in winter; and more anticyclonic eddies (AEs) in summer. He et al. (2002) found that eddy kinetic energy (EKE) exists distinct seasonal variability in the northeastern SCS, which is higher in boreal winter than in summer. Wang et al. (2006) pointed out that more than half of the eddies were formed during winter monsoon and were generated in the eastern SCS and off the Vietnam coast. Warm-core eddies northwest of Luzon Island are a seasonal feature that usually appear during summer (Li et al., 1998; Yuan et al., 2007; Chen et al., 2010), and cold-core eddies northwest of Luzon Island usually appear in winter (Shaw et al., 1996; Yang and Liu, 2003; Wang et al., 2008a).

1.2 *Generation mechanisms of mesoscale eddies in the eastern SCS*

Instability of mean flow can generate eddies west of the Luzon Strait, especially during the Kuroshio intrusion (Wang et al., 2000; Su, 2004; Wang et al., 2008b). But the mean flow in the eastern SCS (ESCS; 11°–18°N, 114°–120°E) is relatively weak that could not provide enough energy for the eddy generation. The generation mechanisms of the eddies in the ESCS are still controversial. Several studies have pointed out that eddies in the ESCS are related to the local wind stress curl. For example, eddies in the northeastern SCS are attributed to wind stress curl variation, and the Luzon Cold Eddy acts as a forced Rossby wave (Yang and Liu, 2003). The winter orographic wind jets are involved in the

Foundation item: The National Natural Science Foundation of China under contract Nos 41522601, 41876002, 41876224 and 4170060064; the Fundamental Research Funds for the Central Universities under contract Nos 2017B04714 and 2017B4114.
*Corresponding author, E-mail: xuhuacheng@hhu.edu.cn

generation of eddies northwest and west of Luzon Island (Wang et al., 2005; Wang et al., 2008a). Wang et al. (2005) defined the winter as the period from October to the following March, as there is winter monsoon during the period. They found that the eddies detected from the altimetry data correspond well with local wind stress curl in the ESCS during winter. However, the wind forcing could not explain all the eddies in the ESCS, especially during summer when the wind stress is relatively weak.

Hu et al. (2001), Zheng et al. (2011) and Hu et al. (2012) suggested that eddies generated by the nonlinearity of Rossby waves from the WTP can propagate into the SCS via the Luzon Strait. However, these kind of eddies always propagate along the continental slope and hardly enter into the ESCS.

Recently, Nan et al. (2011) detected three long-lived, warm-core eddies in the northern SCS during August 2007 based on both altimetry data and *in situ* measurements along 18°N. Such eddies were also observed in summer 2009. Zheng et al. (2014) utilized an intrinsic standing wave mode to explain the formation of these three long-lived eddies. The theoretical standing wave mode coincides well with the seiche events observed by the cruise mission in summer 2007 and 2009. It is worth noting that the nonlinear effect is crucial for the generation of eddies (Hurlburt and Thompson, 1980; Wang et al., 2006). According to Chelton et al. (2011), about 90% of the observed mesoscale eddies in the tropics (20°S–20°N) are nonlinear. Therefore, linear theory cannot fully explain the generation of mesoscale eddies in the SCS, also in the ESCS.

Recent studies suggested that the coastal trapped waves (CTWs) originated from the WTP traveling clockwise along the coast of Luzon Island through the Sibutu Passage and Mindoro Strait can radiate westward Rossby waves on the west coast of Luzon Island and impact sea surface height variation (Liu et al., 2011; Zhuang et al., 2013; Chen et al., 2015; Cheng et al., 2016). The instability of the baroclinic Rossby waves radiated from the west coast of Luzon Island may be another generation mechanism for the eddies in the ESCS, which may be affected by the remote forcing from WTP.

1.3 *Our view and approach*

The purpose of the present paper is to reveal dynamic processes for mesoscale eddy generation in the ESCS, which remain controversial as mentioned in Section 1.2. We propose that eddies derive their energy from wind forcing and baroclinic Rossby waves, which are radiated from the poleward CTWs along the west coast of Luzon Island. The paper is organized as follows. In Section 2, we introduce the data and methods used in this study. In Section 3, we describe the features of mesoscale eddies in the ESCS using satellite observations. In Section 4, we investigate the essential dynamic process for eddy formation based on a nonlinear, 1½-layer reduced-gravity model, hereinafter referred to as 1½-layer model. In Section 5, summary is given.

2 Data and model

2.1 *Altimetry data and wind data*

The sea surface height anomaly (SSHA) data from a merged product of altimeter observations by multiple satellites (TOPEX/Poseidon and ERS, followed by Jason-1/2 and Envisat) are used to describe the main features of the eddies in the SCS. The data are distributed by the Archiving, Validation and Interpretation of Satellite Oceanographic data (AVISO http://www.aviso.oceanobs.com/), available on 0.25° grid at daily interval. A tidal model GOT2000 and a barotropic model MOG2D-G were applied to remove the aliasing of tides and barotropic variability (Volkov et al., 2007; Dibarboure et al., 2008). In this study, we select the SSHA data from 1993 to 2013 at 5-d interval.

Sea surface wind data used in this study is daily, 0.75°×0.75° wind stress derived from the European Centre for Medium-Range Weather Forecasts (ECMWF; Dee et al., 2011). It covers the study period.

2.2 *Eddy detection*

Gridded SSHA and geostrophic current velocity from altimetry observations and solutions of a nonlinear, 1½-layer model are used to identify and track mesoscale eddies in the SCS. The automatic winding angle (WA) method (Sadarjoen and Post, 2000; Chaigneau et al., 2008) and eddy tracking algorithm used by Penven et al. (2005) are adopted to identify and track eddies based on filtered SSHA and geostrophic current field. We first find the local maximum (minimum) SSHA in a moving window of 2°×2° as a possible anticyclonic (cyclonic) eddy center. Then, we use the WA method to find the enclosed streamlines in the geostrophic current field, and the outmost enclosed streamline is regarded as the eddy edge. For more details on eddy identification and tracking, readers are referred to Chen et al. (2011). Eddies with lifetime $\geqslant$30 d are saved to estimate eddy locations and properties in this study.

2.3 *The nonlinear, 1½-layer model*

In this paper, we adopt a nonlinear, 1½-layer model to investigate contributions of wind forcing and nonlinear instability of Rossby waves to the formation and modulation of the mesoscale eddies. Previous studies have shown that the 1½-layer model contains essential dynamics of a wind-forced, upper-ocean layer, and has been used to study upper-ocean circulation, sea-level fluctuation, and mesoscale eddies in the SCS (Metzger and Hurlbert, 1996; Liu et al., 2001; Wang et al., 2006, 2010; Zhuang et al., 2013). Following Qiu and Chen (2012), we write down the governing equations as follows:

$$\frac{\partial \boldsymbol{u}}{\partial t} + \zeta \boldsymbol{k} \times \boldsymbol{u} = -\nabla E + A_{\mathrm{h}} \nabla^2 \boldsymbol{u} + \frac{\boldsymbol{\tau}}{\rho_0 h}, \tag{1a}$$

$$\frac{\partial h}{\partial t} + \nabla \cdot (h\boldsymbol{u}) = 0, \tag{1b}$$

where $\boldsymbol{u} = (u, v)$ is the horizontal velocity vector, $\boldsymbol{\tau} = (\tau^x, \tau^y)$ is the wind-stress vector, h is the upper-layer thickness, ρ_0 is the reference density, and A_{h}= 100 m^2/s is the coefficient of horizontal eddy viscosity. Near the boundaries of the model, A_{h} is increased linearly from 100 to 5 000 m^2/s for the purpose of suppressing instabilities and outcropping. $\zeta = f + \boldsymbol{k} \cdot \nabla \times \boldsymbol{u}$ is the absolute vorticity, $E = g'h + \left(u^2 + v^2\right)/2$ is the total energy, and g'=0.036 m/s^2 is the reduced-gravity constant. We set the background layer thickness h_0=250 m. The 200 m isobath is defined as the land/sea boundary, which allows CTWs to pass through the Sibutu Passage and Mindoro Strait. Model sea level is then given by $SSH = (g'/g)\, h$, where g=9.8 m/s^2 is the gravitational constant.

The model domain is 60°S–65°N, 30°E–70°W; and the horizontal resolution is 0.125°×0.125°. The wind forcing from the ECMWF wind stress is interpolated to 0.125°×0.125° resolution and 5-d interval. The model is first spun up with climatological monthly wind stress from the ECMWF for 20 years, and the solutions are taken as the initial conditions for our sensitive experiments.

3 Mesoscale variability based on altimetry data

3.1 *Mesoscale variability*

The SSHA field shows multi-scale features spatially. The mesoscale eddies have a diameter of about 100–500 km (Tansley et al., 2001), so a 100–500 km band-pass-filter is used to extract mesoscale variability. Figure 1 shows the seasonal mean pattern of the band-pass-filtered SSHA from the altimetry data. There exist several alternating positive and negative SSHA bands with a meridional scale of about 2.5°, and the corresponding geostrophic zonal velocity is about 8 cm/s. The opposite patterns between winter and summer indicate that the band-pass-filtered SSHA has distinct seasonal variability. We assume it is the meridional pattern of eddy distribution (e.g., CEs–AEs–CEs from north to south) and special propagation paths that produce the alternating positive and negative bands, and this kind of eddies have obvious annual cycle. For example, positive wind stress curl (WSC) causes CEs northwest of the Luzon Island during winter which propagate westward, leading to negative SSHA; analogously, negative WSC generates AEs, leading to positive SSHA south of the positive WSC. The WSC pattern is reversed during summer, resulting in an opposite SSHA pattern.

Figure 2 shows the amplitude spectra of the SSHA averaged within two subregions, Region 1 (R1 for short; Fig. 2a) and Region 2 (R2; Fig. 2b). In R1, the unfiltered SSHA (black line) has very strong annual variation, which is weakened significantly after band-pass-filtering (red line), as shown in Fig. 2a. This change is understandable since the annual signals in the SCS mainly present basin and subbasin-scale variability, which would be weakened after using a spatial filter on SSHA. The annual variation in R2 is weaker than that in R1, suggesting weaker seasonal wind in R2. However, mesoscale eddies mainly cause local SSHA intraseasonal variability. It is better to use a temporal filter to exclude other mesoscale variability, such as the signals with distinct annual cycle. Therefore, we apply a 30–150-d band-pass-filter to both SSHA and geostrophic current velocity after the spatial band-pass-filter. The results will be used to identify and track mesoscale eddies in the ESCS.

3.2 *Eddy characteristics*

A total of 81 (73) AEs (CEs) are identified within the ESCS (11°–18°N, 114°–120°E; see the green box in Fig. 1) during 1993–2013 from satellite observations, which is about 29% (28%) of the AEs (CEs) generated in the SCS (8°–23°N, 105°–120°E). The eddies generally have a mean lifetime of around 50 d and a mean radius of about 100 km. The mean vorticity is -8.4×10^{-7} s^{-1} for the AEs, and 6.4×10^{-6} s^{-1} for the CEs. Figure 3 shows the tracks of these eddies. The magenta indicates the number of AEs and their tracks, and the blue indicates the number of CEs and their tracks. There is no significant difference between the numbers of the AEs and CEs in the ESCS, and there is no significant seasonal difference because the annual signals were removed before the eddies were identified (figures not shown).

4 Model results

4.1 *Model validation*

Most of the mesoscale eddies in the SCS are caused by wind stress curl, the instability of mean flow, and nonlinear, unstable,

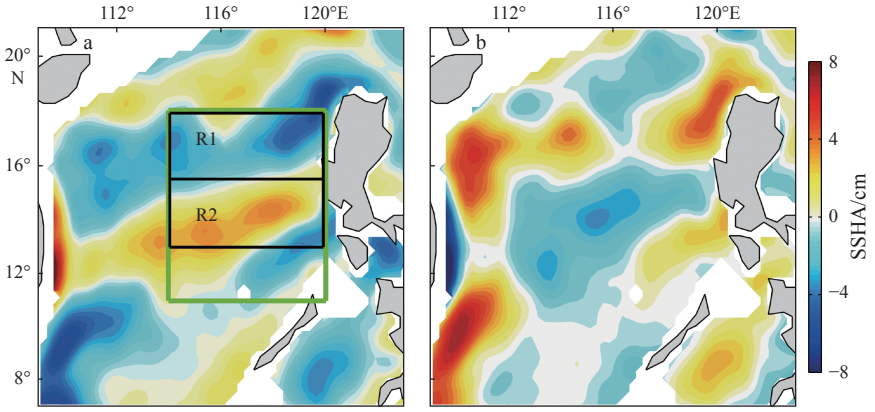

Fig. 1. The seasonal mean band-pass-filtered SSHA in winter (December, January and February) (a) and summer (June, July and August) (b) derived from the altimetry data. The two black boxes (R1, R2) indicate the subregions of the ESCS (11°–18°N, 114°–120°E; green box).

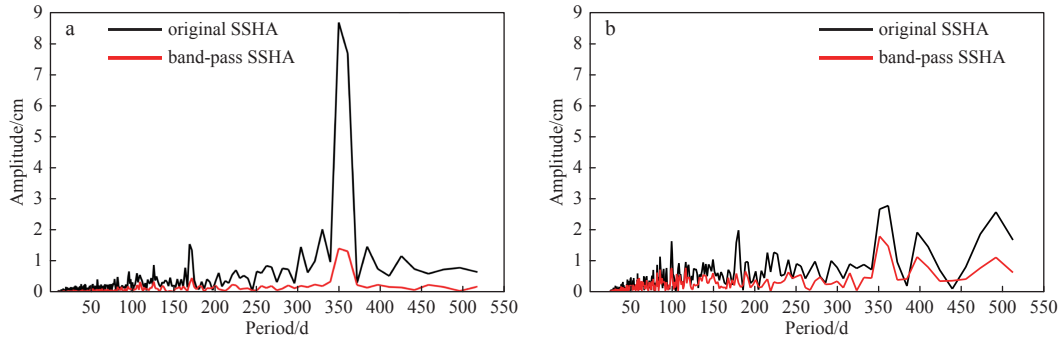

Fig. 2. Amplitude spectra of the SSHA averaged within R1 (a) and R2 (b). The two regions are shown in Fig. 1a. The black curve indicates SSHA and the red curve indicates the SSHA after being filtered at 100–500 km scale.

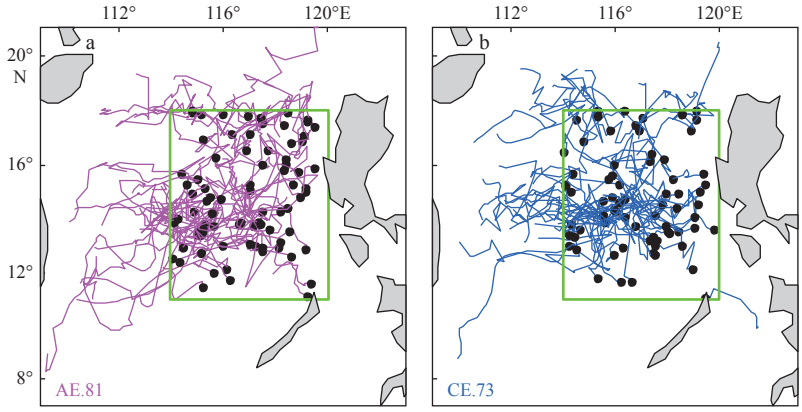

Fig. 3. Tracks of the eddies generated in the ESCS detected from altimeter observations. a. Magenta indicates the tracks of anticyclonic eddies, and b. blue shows the tracks of cyclonic eddies. Black dots mark eddy generation sites.

baroclinic Rossby waves. Since the generation mechanisms of the eddies generated in the ESCS are not well understood, we design a series of numerical experiments to investigate the relative roles of the wind forcing in the interior SCS (8°–23°N, 105°–120°E, Box 1; Fig. 4) and the remote forcing from the WTP (5°–20°N, 125°E–90°W, Box 2; Fig. 4) in eddy generation in the ESCS. Each experiment is forced by modified wind stress at 5-d interval from 1979 to 2013, but we only analyze the period of 1993–2013. The configurations of all experiments are listed in Table 1, and will be introduced one by one as needed.

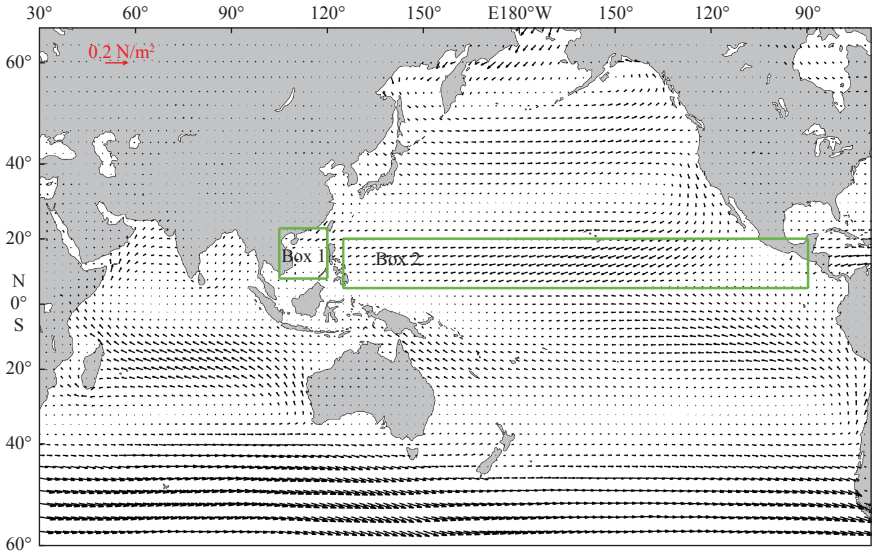

Fig. 4. Distribution of time-mean wind stress from ECMWF. The time mean is taken from the period of 1993–2013. The two boxes are used for sensitive experiments representative for the SCS and the WTP.

Experiment 0 as the control run is forced by realistic 5-d wind stress. Figure 4 shows the mean state of the wind stress. As shown in Fig. 5, seasonal mean pattern of the 100–500 km band-pass-filtered SSHA in Exp. 0 matches quite well with that from the observations (Fig. 1). They all show distinct features, namely, alternating positive and negative SSHA bands, with significant seasonal variability and strong western boundary current.

Table 1. The configurations of 1½-layer model experiments

Experiment	Wind forcing
Exp. 0	control run, real wind forcing
Exp. 1	300-d low-pass-filtered wind forcing
Exp. 2	real wind forcing in Box 1, same forcing as Exp. 1 in other regions
Exp. 3	real wind forcing in Box 2, same forcing as Exp. 1 in other regions
Exp. 4	remove the wind in Box 1, same forcing as Exp. 1 in other regions
Exp. 5	remove the wind in Box 2, same forcing as Exp. 1 in other regions

The tracks of the eddies detected from Exp. 0 are plotted in Fig. 6. A total of 90 (79) AEs (CEs) are identified in the ESCS. The numbers of AEs (CEs) is almost 30% (26%) of AEs (CEs) generated in the SCS, which is very close to the 29% (28%) from the observations. The mean lifetime is around 80 d, and the mean radius is about 120 km, both of which are larger than those from the observations (Table 2). This difference from observations may be due to the coefficient of horizontal eddy viscosity being small, and to the fact that the baroclinic instability is weak in the 1½-layer model. The mean vorticity is -9.6×10^{-7} s^{-1} for the AEs, and 4.0×10^{-6} s^{-1} for the CEs in the ESCS.

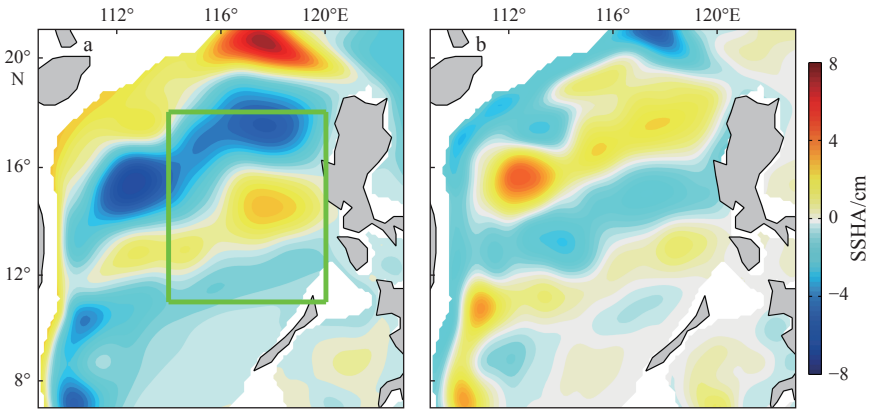

Fig. 5. Seasonal mean band-pass-filtered SSHA in winter (December, January and February) (a) and summer (June, July and August) (b) derived from Exp. 0.

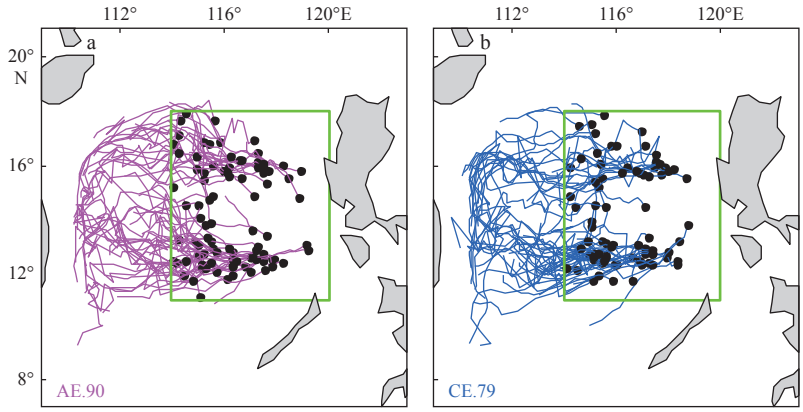

Fig. 6. Tracks of the eddies generated in the ESCS detected from Exp. 0. a. Magenta indicates the tracks of anticyclonic eddies, and b. blue shows the tracks of cyclonic eddies. Black dots mark eddy generation sites.

Table 2. Main features of eddies generated in the ESCS

	Numbers (AEs+CEs)	Lifetime/d	Radius/km	Vorticity (AE)/10^{-7} s^{-1}	Vorticity (CE)/10^{-6} s^{-1}
Observation	154	47	103	–8.4	6.4
Exp. 0	169	80	117	–9.6	4.0
Exp. 1	25	82	127	–8.5	3.3

4.2 *Eddy generation mechanisms*

Several studies suggested that the winter orographic wind jet is a key mechanism for the eddy generation in the ESCS (e.g., Wang et al., 2005, 2008a). However, the orographic wind is relatively weak during summer and could not explain the generation of eddies generated in the ESCS in summer. We assume that the high-frequency wind plays an important role in eddy generation, which unfortunately is wiped out after seasonal averaging. Therefore, we will examine the relative roles of the low-frequency wind and high-frequency wind in eddy generation in the ESCS using model experiments. We design Exps 1–3 with different wind forcing. Forcing in Exp. 1 is the low-frequency wind stress obtained by using a 300-d low-pass-filter. Less mesoscale eddies are seen in Exp. 1 (Fig. 7), and the number of the eddies is about 15% (25/169) of that in Exp. 0 (control run; Table 3). This tells us that the low-frequency SCS wind forcing does not generate many eddies. Can the high-frequency wind (300-d high-passed) be important for generating eddies in the ESCS? If the low-frequency wind is replaced by the real wind in the SCS region (Box 1; Fig. 4) in Exp. 2, it reproduces about 69% (116/169) of the eddies in Exp. 0. When the low-frequency wind is replaced by the real wind in the WTP (Box 2; Fig. 4) in Exp. 3, it reproduces about 55% (93/169) of the eddies in the ESCS (Table 3). In all these experiments, the modified winds are smoothed along the segment boundaries to eliminate sharp discontinuities. Therefore, besides the wind forcing in the interior SCS, the signals from the WTP forced by high-frequency wind are another important forcing for mesoscale eddy generation in the ESCS.

To estimate the effect of high-frequency wind, we subtract the numbers of eddies of Exp. 1 from those of Exp. 2 or Exp. 3. The results show that the high-frequency (300-day high-passed) wind in Box 1 (Fig. 4) produces about 54% of the eddies in the ESCS, and the high-frequency wind in Box 2 (Fig. 4) produces about 40% of the eddies in the ESCS (Table 4). The sum of the above-mentioned three contributions (15%, 54% and 40%) exceeds 100%, which can be explained by the fact that the model ocean is a nonlinear system.

To further figure out the contributions of the low-frequency wind in Box 1 and in Box 2 (Fig. 4) to the eddy generation in the ESCS, we remove the wind forcing in Box 1 in Exp. 4 and remove

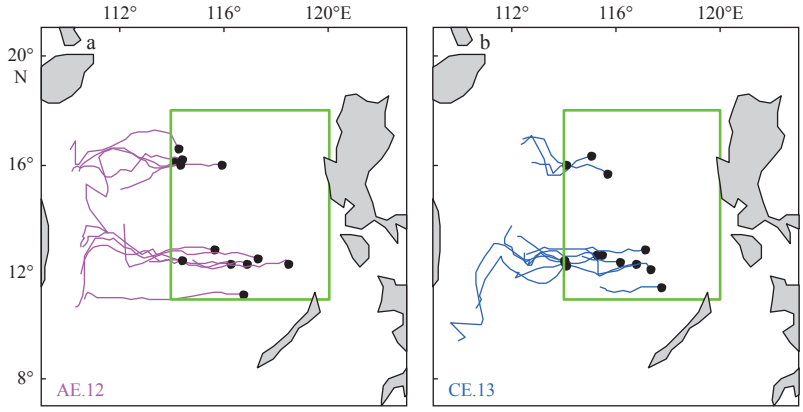

Fig. 7. Tracks of the eddies generated in the ESCS detected from Exp. 1. a. Magenta indicates the tracks of anticyclonic eddies, and b. blue shows the tracks of cyclonic eddies. Black dots mark eddy generation sites.

Table 3. Numbers of eddies generated in the ESCS in various experiments

	Exp. 0	Exp. 1	Exp. 2	Exp. 3	Exp. 4	Exp. 5
Total	169	25	116	93	5	0
Percentage/%	100	15	69	55	3	0

Table 4. Numbers of eddies generated in the ESCS in Exp. 0 and Exp. 1, and the differences of Exp. 2 minus Exp. 1 and of Exp. 3 minus Exp. 1

	Exp. 0 (total)	Exp. 1	Exp. 2–Exp. 1	Exp. 3–Exp. 1
Difference	169	25	91	68
Percentage/%	100	15	54	40

the wind forcing in Box 2 in Exp. 5. In the other regions, the wind forcing is the same as in Exp. 1. Experiment 4 produces merely five eddies, while no eddy is produced in Exp. 5, as shown in Table 3. These results suggest that the signals that are only driven by the low-frequency wind over the interior SCS are not enough to generate mesoscale eddies in the ESCS, while they could produce mesoscale eddies only when there is wind forcing in the WTP.

Signals from the WTP travel clockwise along the coast of Luzon Island via the Sibutu Passage and Mindoro Strait (Liu et al., 2011; Zhuang et al., 2013; Cheng et al., 2016). The coastal Kelvin waves can stimulate Rossby waves from the west coast of Luzon Island, which may affect the eddy generation in the ESCS. To confirm that the signals from the WTP could enter the west of Luzon Island, and to explore their impact on eddy generation in the ESCS, we obtain the evolution of SSHA via regression analysis. Since the high-frequency signals from the WTP can easily generate eddies in the ESCS, as illustrated in Section 4.2 (Exp. 3), we employ the 300-d high-pass-filtered SSHA from Exp. 0 to estimate the propagation of the signals from the WTP.

Figure 8 displays the evolution of filtered SSHA via regression analysis. The SSHA reference site is off the west coast of Luzon Island at (13.0°–13.5°N, 120.0°–120.5°E). At –50 d (Fig. 8a), a positive SSHA signal appears southeast of the Philippines, and encounters the coast of the Philippines. The positive signal propagates clockwise along the coast as CTWs. Ten days later (Fig. 8b), the SSHA phase along the west coast of Luzon Island rapidly turns to be positive, and then gets enhanced (Figs 8c and d). Once departed from the coast, the strong positive SSHA contour may become enclosed (Figs 8e–l). The enclosed SSHA may devel-

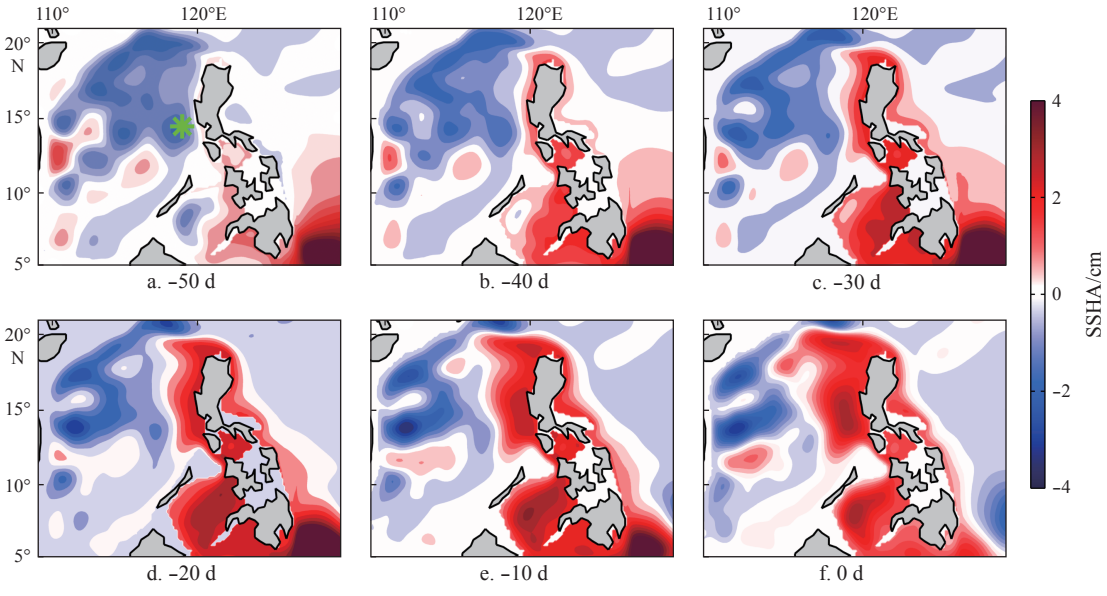

Fig. 8.

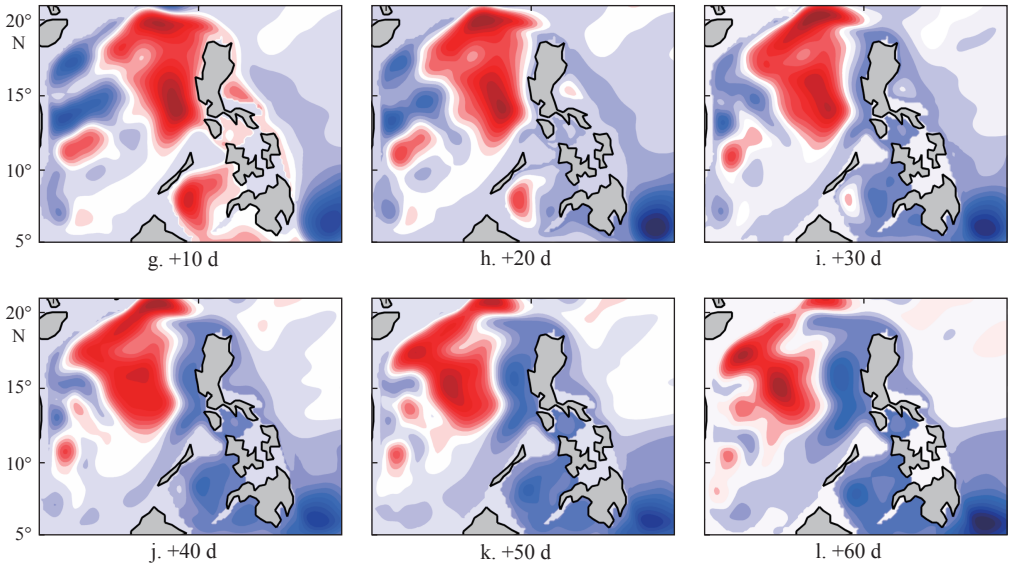

Fig. 8. Lead-lag regression of the 300-d high-pass-filtered SSHA from Exp. 0 after having normalized the 300-d high-pass-filtered SSHA within the reference box (13.0°–13.5°N, 120.0°–120.5°E; the green star in a).

op into mesoscale AE and propagate westward. There appears a negative SSHA signal southeast of the Philippines two months later (Fig. 8h), which evolves in the same way as the previous positive signal.

The evolution reveals that the equatorial-originated signals excite the CTWs after reaching the coast, which can radiate Rossby waves equatorward of the critical latitude (Clarke, 1983; Clarke and Shi, 1991). These signals are quite to mesoscale eddy generation in the ESCS. The Rossby waves become unstable, and turn into individual eddies at certain distance from the west coast

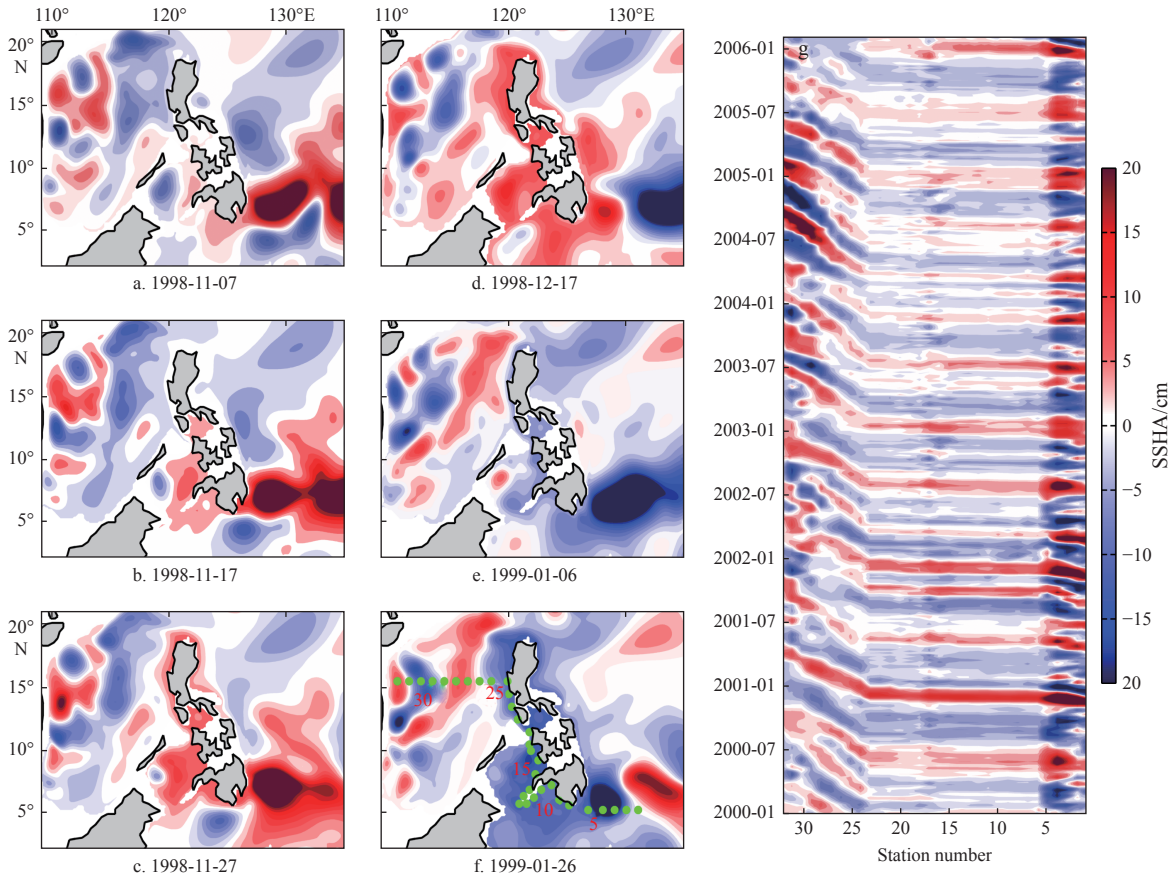

Fig. 9. Snapshots of the 300-d high-pass-filtered SSHA from Exp. 0 (a–f), and corresponding time-station diagram of the 300-d high-pass-filtered SSHA from Exp. 0 (g). The waveguide is noted by green dots.

of Luzon Island. Figure 9 shows the snapshots of the 300-d high-pass-filtered SSHA from Exp. 0, demonstrating that the signals from the WTP indeed propagate into the SCS as the CTWs. We select one typical waveguide shown by the green dots in Fig. 9f to explore the evolution of the signals, where the numbers in red indicate the station sequence. The signals propagate clockwise as the CTWs with a speed of about 2.2 m/s (from Sta. 6 to Sta. 23), which agrees with the phase speed of the first-mode gravity wave at this latitude, about 2.6–2.8 m/s (Chelton et al., 1998). Then, the signals propagate westward with a speed of about 0.12 m/s (after Sta. 23), which is close to the first-mode baroclinic Rossby wave (about 0.11 m/s).

5 Summary

In this paper, we show the distribution of the eddies generated in the ESCS and explore the eddy formation mechanisms using altimeter observations and a nonlinear, 1½-layer model. Eddies in the ESCS have a mean lifetime of around 50 d and a mean radius of about 100 km. Both the observations and the solutions of 1½-layer model show that there exist several alternating positive and negative SSHA bands with a meridional scale of about 2.5°. The patterns are reversed between winter and summer. This implies that the 1½-layer model can capture the essential physics of upper-ocean sea surface height and mesoscale variability in the ESCS.

To estimate the contributions of local wind forcing in the interior SCS and remote wind forcing from the WTP to the eddy generation in the ESCS, we design several sensitive experiments by forcing the 1½-layer model with modified wind. The solutions suggest that the contribution of local wind forcing in the interior SCS and the signals from the WTP are comparable. The high-frequency wind forcing in the interior SCS can explain almost 54% of the mesoscale eddies in the ESCS from control run, while the signals from the WTP can explain about 40% of the mesoscale eddies in the ESCS from control run. Although such a linear decomposition cannot give an accurate evaluation of the nonlinear dynamics involved in the eddy generation in this model, this approach can provide useful insight of the physical processes involved and help us better understand the relative roles of different wind forcing.

To figure out the dynamic process involved in the signals from the WTP that influence the eddy generation in the ESCS, we conduct a regression analysis of 300-d high-pass-filtered SSHA from Exp. 0. In addition, we choose a typical waveguide to confirm the evolution of the signals. All the results show that the wind-forced signals from the WTP do propagate into the SCS as the CTWs. The Rossby waves radiated from the west coast of Luzon Island may become unstable and turn into individual eddies.

Acknowledgements

AVISO sea level data were obtained from http://www.aviso.altimetry.fr/en/data/dataaccess.html and ERA-Interim (ERA-I) surface wind-speed data from the European Centre for Medium-Range Weather Forecasts (ECMWF) product were obtained from http://www.ecmwf.int/products/data/archive/. The authors express appreciation to AVISO and ECMWF for providing data.

References

Chaigneau A, Gizolme A, Grados C. 2008. Mesoscale eddies off Peru in altimeter records: Identification algorithms and eddy spatio-temporal patterns. Progress in Oceanography, 79(2–4): 106–119, doi: 10.1016/j.pocean.2008.10.013

Chelton D B, Deszoeke R A, Schlax M G, et al. 1998. Geographical variability of the first baroclinic rossby radius of deformation. Journal of Physical Oceanography, 28(3): 433–460, doi: 10.1175/1520-0485(1998)028<0433:GVOTFB>2.0.CO;2

Chelton D B, Schlax M G, Samelson R M. 2011. Global observations of nonlinear mesoscale eddies. Progress in Oceanography, 91(2): 167–216, doi: 10.1016/j.pocean.2011.01.002

Chen Gengxin, Hou Yijun, Chu Xiaoqing. 2011. Mesoscale eddies in the South China Sea: Mean properties, spatiotemporal variability, and impact on thermohaline structure. Journal of Geophysical Research: Oceans, 116(C6): C06018, doi: 10.1029/2010JC006716

Chen Xiao, Qiu Bo, Cheng Xuhua, et al. 2015. Intra-seasonal variability of Pacific-origin sea level anomalies around the Philippine Archipelago. Journal of Oceanography, 71(3): 239–249, doi: 10.1007/s10872-015-0281-9

Cheng Xuhua, Qi Yiquan. 2010. Variations of eddy kinetic energy in the South China Sea. Journal of Oceanography, 66(1): 85–94, doi: 10.1007/s10872-010-0007-y

Cheng Xuhua, Xie Shangping, Du Yan, et al. 2016. Interannual-to-decadal variability and trends of sea level in the South China Sea. Climate Dynamics, 46(9–10): 3113–3126, doi: 10.1007/s00382-015-2756-1

Clarke A J. 1983. The reflection of equatorial waves from oceanic boundaries. Journal of Physical Oceanography, 13(7): 1193–1207, doi: 10.1175/1520-0485(1983)013<1193:TROEWF>2.0.CO;2

Clarke A J, Shi Chuan. 1991. Critical frequencies at ocean boundaries. Journal of Geophysical Research: Oceans, 96(C6): 10731–10738, doi: 10.1029/91JC00933

Dee D P, Uppala S M, Simmons A J, et al. 2011. The ERA-Interim reanalysis: configuration and performance of the data assimilation system. Quarterly Journal of the Royal Meteorological Society, 137(656): 553–597, doi: 10.1002/qj.v137.656

Dibarboure G, Lauret O, Mertz F, et al. 2008. SSALTO/DUACS User Handbook: (M)SLA and (M)ADT Near-Real Time and Delayed Time Products, Rep. CLS-DOS-NT-06. 034, Ramonville St. Agne, France: Aviso Altimetry

Fang Guohong, Fang Wendong, Fang Yue, et al. 1998. A survey of studies on the South China Sea upper ocean circulation. Acta Oceanographica Taiwanica, 37(1): 1–16

He Zhigang, Wang Dongxiao, Hu Jianyu. 2002. Features of eddy kinetic energy and variations of upper circulation in the South China Sea. Acta Oceanologica Sinica, 21(2): 305–314

Hu Jianyu, Kawamura H, Hong Huasheng, et al. 2001. 3–6 Months variation of sea surface height in the South China Sea and its adjacent ocean. Journal of Oceanography, 57(1): 69–78, doi: 10.1023/A:1011126804461

Hu Jianyu, Zheng Quanan, Sun Zhenyu, et al. 2012. Penetration of nonlinear Rossby eddies into South China Sea evidenced by cruise data. Journal of Geophysical Research: Oceans, 117(C3): C03010

Hurlburt H E, Thompson J D. 1980. A numerical study of loop current intrusions and eddy shedding. Journal of Physical Oceanography, 10(10): 1611–1651, doi: 10.1175/1520-0485(1980)010<1611:ANSOLC>2.0.CO;2

Hwang C, Chen S A. 2000. Circulations and eddies over the South China Sea derived from TOPEX/Poseidon altimetry. Journal of Geophysical Research: Oceans, 105(10): 23943–23965

Li Li, Nowlin W D Jr, Su Jilan. 1998. Anticyclonic rings from the Kuroshio in the South China Sea. Deep Sea Research Part I: Oceanographic Research Papers, 45(9): 1469–1482, doi: 10.1016/S0967-0637(98)00026-0

Liu Qinyan, Feng Ming, Wang Dongxiao, et al. 2011. ENSO-induced interannual variability in the southeastern South China Sea. Journal of Oceanography, 67(1): 127–133, doi: 10.1007/s10872-011-0002-y

Liu Qinyu, Kaneko A, Su Jilan. 2008. Recent progress in studies of the South China Sea circulation. Journal of Oceanography, 64(5): 753–762, doi: 10.1007/s10872-008-0063-8

Liu Zhengyu, Yang Haijun, Liu Qinyu. 2001. Regional dynamics of

seasonal variability in the South China Sea. Journal of Physical Oceanography, 31(1): 272–284, doi: 10.1175/1520-0485(2001)031<0272:RDOSVI>2.0.CO;2

Metzger E J, Hurlburt H E. 1996. Coupled dynamics of the South China Sea, the Sulu Sea, and the Pacific Ocean. Journal of Geophysical Research: Oceans, 101(C5): 12331–12352, doi: 10.1029/95JC03861

Nan Feng, He Zhigang, Zhou Hui, et al. 2011. Three long-lived anticyclonic eddies in the northern South China Sea. Journal of Geophysical Research: Oceans, 116(C5): C05002, doi: 10.1029/2010JC006790

Penven P, Echevin V, Pasapera J, et al. 2005. Average circulation, seasonal cycle, and mesoscale dynamics of the Peru Current System: A modeling approach. Journal of Geophysical Research: Oceans, 110(C10): C10021, doi: 10.1029/2005JC002945

Qiu Bo, Chen Shuiming. 2012. Multidecadal sea level and gyre circulation variability in the northwestern tropical Pacific Ocean. Journal of Physical Oceanography, 42(1): 193–206, doi: 10.1175/JPO-D-11-061.1

Qu Tangdong. 2000. Upper-layer circulation in the South China Sea. Journal of Physical Oceanography, 30(6): 1450–1460, doi: 10.1175/1520-0485(2000)030<1450:ULCITS>2.0.CO;2

Sadarjoen I A, Post F H. 2000. Detection, quantification, and tracking of vortices using streamline geometry. Computers & Graphics, 24(3): 333–341

Shaw P T, Chao S Y, Liu K K, et al. 1996. Winter upwelling off Luzon in the northeastern South China Sea. Journal of Geophysical Research: Oceans, 101(C7): 16435–16448, doi: 10.1029/96JC01064

Su Jilan. 2004. Overview of the South China Sea circulation and its influence on the coastal physical oceanography outside the Pearl River estuary. Continental Shelf Research, 24(16): 1745–1760, doi: 10.1016/j.csr.2004.06.005

Tansley C E, Marshall D P. 2001. Flow past a Cylinder on a β Plane, with application to gulf stream separation and the Antarctic circumpolar current. Journal of Physical Oceanography, 31(11): 3274–3283, doi: 10.1175/1520-0485(2001)031<3274:FPACOA>2.0.CO;2

Volkov D L, Larnicol G, Dorandeu J. 2007. Improving the quality of satellite altimetry data over continental shelves. Journal of Geophysical Research, 112(C6): C06020, doi: 10.1029/2006JC003765

Wang Guihua, Chen Dake, Su Jilan. 2006. Generation and life cycle of the dipole in the South China Sea summer circulation. Journal of Geophysical Research: Oceans, 111(C6): C06002, doi: 10.1029/2005JC003314

Wang Guihua, Chen Dake, Su Jilan. 2008a. Winter eddy genesis in the eastern South China Sea due to orographic wind jets. Journal of Physical Oceanography, 38(3): 726–732, doi: 10.1175/2007JPO3868.1

Wang Liping, Koblinsky C J, Howden S. 2000. Mesoscale variability in the South China Sea from the TOPEX/Poseidon altimetry data. Deep Sea Research Part I: Oceanographic Research Papers, 47(4): 681–708, doi: 10.1016/S0967-0637(99)00068-0

Wang Guihua, Su Jilan, Chu P C. 2003. Mesoscale eddies in the South China Sea observed with altimeter data. Geophysical Research Letters, 30(21): 2121, doi: 10.1029/2003GL018532

Wang Guihua, Su Jilan, Li Rongfeng. 2005. Mesoscale eddies in the South China Sea and their impact on temperature profiles. Acta Oceanologica Sinica, 24(1): 39–45

Wang Guihua, Wang Chunzai, Huang Ruixin. 2010. Interdecadal variability of the eastward current in the South China Sea associated with the Summer Asian monsoon. Journal of Climate, 23(22): 6115–6123, doi: 10.1175/2010JCLI3607.1

Wang Dongxiao, Xu Hongzhou, Lin Jing, et al. 2008b. Anticyclonic eddies in the northeastern South China Sea during winter 2003/2004. Journal of Oceanography, 64(6): 925–935, doi: 10.1007/s10872-008-0076-3

Wyrtki K. 1961. Physical Oceanography of the Southeast Asian Waters. Naga Rep, 2, Scripps Institution of Oceanography. San Diego: University of California

Xiu Peng, Chai Fei, Shi Lei, et al. 2010. A census of eddy activities in the South China Sea during 1993-2007. Journal of Geophysical Research: Oceans, 115(C3): C03012, doi: 10.1029/2009JC005657

Yang Haijun, Liu Qinyu. 2003. Forced Rossby wave in the northern South China Sea. Deep Sea Research Part I: Oceanographic Research Papers, 50(7): 917–926, doi: 10.1016/S0967-0637(03)00074-8

Yuan Dongliang, Han Weiqing, Hu Dunxin. 2007. Anti-cyclonic eddies northwest of Luzon in summer-fall observed by satellite altimeters. Geophysical Research Letters, 34(13): L13610, doi: 10.1029/2007GL029401

Zheng Quanan, Hu Jianyu, Zhu Benlu, et al. 2014. Standing wave modes observed in the South China Sea deep basin. Journal of Geophysical Research: Oceans, 119(7): 4185–4199, doi: 10.1002/2014JC009957

Zheng Quanan, Tai Changkuo, Hu Jianyu, et al. 2011. Satellite altimeter observations of nonlinear Rossby eddy-Kuroshio interaction at the Luzon Strait. Journal of Oceanography, 67(4): 365–376, doi: 10.1007/s10872-011-0035-2

Zhuang Wei, Qiu Bo, Du Yan. 2013. Low-frequency western Pacific Ocean sea level and circulation changes due to the connectivity of the Philippine Archipelago. Journal of Geophysical Research: Oceans, 118(12): 6759–6773, doi: 10.1002/2013JC009376

Zhuang Wei, Xie Shangping, Wang Dongxiao, et al. 2010. Intraseasonal variability in sea surface height over the South China Sea. Journal of Geophysical Research: Oceans, 115(C4): C04010, doi: 10.1029/2009JC005647

Zu Tingting, Wang Dongxiao, Yan Changxiang, et al. 2013. Evolution of an anticyclonic eddy southwest of Taiwan. Ocean Dynamics, 63(5): 519–531, doi: 10.1007/s10236-013-0612-6